7764–7777 Nucleic Acids Research, 2010, Vol. 38, No. 21 Published online 17 July 2010
doi:10.1093/nar/gkq586

Structure and function of the regulatory HRDC domain from human Bloom syndrome protein

Young Mee Kim and Byong-Seok Choi*

Department of Chemistry, KAIST, Daejon 305-701, Korea

Received March 23, 2010; Revised June 8, 2010; Accepted June 9, 2010

ABSTRACT

The helicase and RNaseD C-terminal (HRDC) domain, conserved among members of the RecQ helicase family, regulates helicase activity by virtue of variations in its surface residues. The HRDC domain of Bloom syndrome protein (BLM) is known as a critical determinant of the dissolution function of double Holliday junctions by the BLM–Topoisomerase IIIα complex. In this study, we determined the solution structure of the human BLM HRDC domain and characterized its DNA-binding activity. The BLM HRDC domain consists of five α-helices with a hydrophobic 3_{10}-helical loop between helices 1 and 2 and an extended acidic surface comprising residues in helices 3–5. The BLM HRDC domain preferentially binds to ssDNA, though with a markedly low binding affinity (K_d ~100 μM). NMR chemical shift perturbation studies suggested that the critical DNA-binding residues of the BLM HRDC domain are located in the hydrophobic loop and the N-terminus of helix 2. Interestingly, the isolated BLM HRDC domain had quite different DNA-binding modes between ssDNA and Holliday junctions in electrophoretic mobility shift assay experiments. Based on its surface charge separation and DNA-binding properties, we suggest that the HRDC domain of BLM may be adapted for a unique function among RecQ helicases—that of bridging protein and DNA interactions.

INTRODUCTION

Bloom syndrome is a rare hereditary disease characterized by a predisposition to the development of cancer (1). Bloom syndrome cells show an ~10-fold elevation in the frequency of sister-chromatid exchanges, which is caused by mutations in the *BLM* gene (2,3). Bloom syndrome protein (BLM) is one of five human RecQ helicase family members, all of which play critical roles in DNA recombination, replication and repair pathways ranging from bacteria to humans (4,5). The biological importance of the RecQ family is related to three cancer-prone human syndromes—Bloom, Werner and Rothmund–Thompson syndromes—that arise from mutations within the *BLM*, *WRN* and *RECQ4* genes, respectively (3,6,7).

The functional significance of RecQ helicases is that they are DNA-specific enzymes, each binding to a different set of DNA structures. BLM has an apparent preference for DNA substrates containing Holliday junctions, G4 DNA and D-loops (8–10). These are highly related to the cellular functions of BLM, which is involved in the early and late steps of homologous recombination (HR). BLM can catalyze efficient Holliday junction branch migration as an anti-recombinase to prevent genome instability (11–13). BLM is unique among the five human RecQ helicases in that it is able to process a double Holliday junction (dHJ) with Topoisomerase IIIα (TOPOIIIα) (14). In particular, the helicase and RNaseD C-terminal (HRDC) domain of BLM is a critical regulator for dissolution of dHJs by the BLM–TOPOIIIα complex (15).

BLM contains one unique domain and three conserved domains of the RecQ helicase family (Figure 1A). The unique N-terminal domain is not well characterized, but is involved in BLM oligomerization (16) as well as protein–protein interactions, including those with TOPOIIIα (14), Rad51 (17) and RPA (18). The RecQ family is defined by a highly conserved helicase domain that includes seven sequence motifs that are distinct from other helicases. The RQC domain is composed of two subdomains, one of which is a winged-helix domain involved in duplex DNA binding, and the other a Zn^{2+}-binding motif (19–22). The helicase and winged-helix domains combine to form the catalytic core, which is sufficient for ATPase and DNA unwinding activities in *Escherichia coli* RecQ (23), *Saccharomyces cerevisiae* Sgs1 (24) and human BLM (25). C-terminal to the catalytic core, the HRDC domain forms an independent

*To whom correspondence should be addressed. Tel: +82 42 350 2828; Fax: +82 42 350 2858; Email: byongseok.choi@kaist.ac.kr

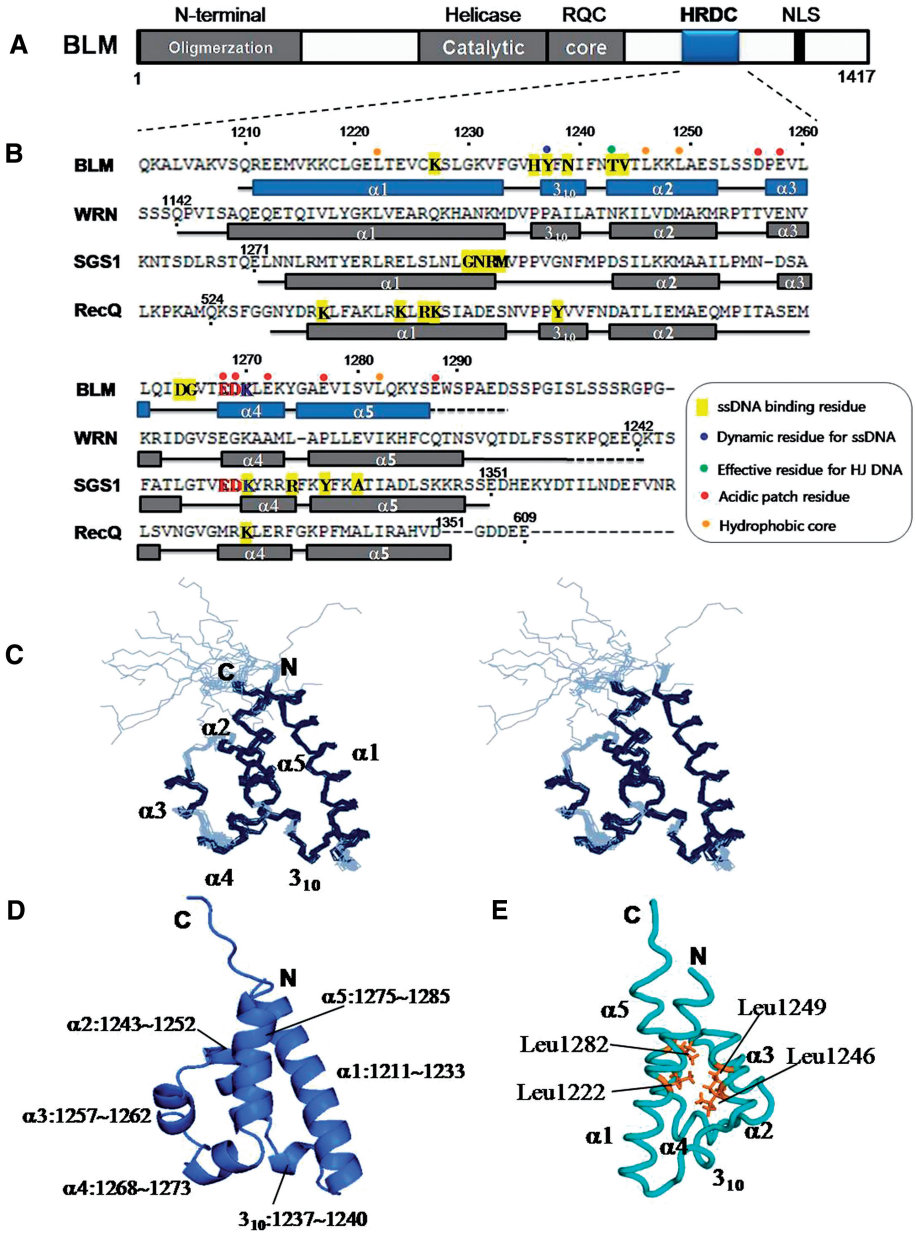

Figure 1. Structure of the human BLM HRDC domain. (**A**) Schematic diagram of conserved domains in full-length BLM: helicase, RQC and HRDC. The N-terminal region is an intrinsic domain for protein–protein interaction and oligomerization of BLM. (**B**) Sequence alignment of the HRDC domain of BLM, WRN, Sgs1 and *E. coli* RecQ based on their 3D structures. Secondary structural elements (helices) are shown below each sequence as blue (BLM, present work) or grey (WRN, SGS1, *E. coli* RecQ) bars. Loop regions are shown as a solid line, whereas the disordered residues at the C-termini of BLM and WRN HRDC are shown as a dashed line. The BLM, Sgs1 and *E. coli* residues that were reported to affect ssDNA binding are highlighted in yellow. The residues of human BLM that affect DNA binding are denoted by blue and green circles, and the residues that contribute to the acidic surface of BLM HRDC are indicated by red circles. A conserved acidic pin motif is indicated with red and blue bold letters. The four residues of the conserved hydrophobic core of HRDC homologues are denoted by orange circles. (**C**) Stereoviews of the ensemble of the 20 lowest-energy NMR structures. (**D**) 3D representative structure of the human BLM HRDC domain in the same orientation as in (C). (**E**) Ribbon diagram of the four residues of the conserved hydrophobic core, Leu1222, Leu1246, Leu1249 and Leu1282, of the human BLM HRDC domain.

helical bundle and might be involved in DNA binding, particularly in conferring some degree of DNA substrate specificity. Of the three conserved sequence elements of the RecQ proteins, the HRDC domain has the lowest sequence identity between family members (26).

The structures of isolated HRDC domains from *E. coli* RecQ (27), *S. cerevisiae* Sgs1 (28), human WRN (29) and *Deinococcus radiodurans* RecQ (DrRecQ) (30), all share a similar overall fold but exhibit distinct functions. For example, the isolated Sgs1 HRDC domain binds to ssDNA and 3′-overhanging duplex structures, whereas the *E. coli* RecQ HRDC binds only to ssDNA. In contrast to unicellular RecQ HRDC domains, which function via auxiliary contacts to DNA, the WRN and BLM HRDC domains have been suggested to mediate diverse molecular interactions via their electrostatic surfaces properties (28).

Actually a recent study showed that the isolated human WRN HRDC domain did not interact with DNA and suggested instead that it mediates protein–protein interactions (29). However, the HRDC domain of BLM is known as a critical determinant for the efficient binding to and unwinding of dHJ DNA by the BLM–TOPOIIIα complex. Furthermore, Lys1270 of the HRDC domain is highly likely to play a role in mediating interactions with DNA (15). A recent study showed that unusual electrostatic surface of the third HRDC domain of DrRecQ (DrRecQ HRDC #3) is important to regulate structure-specific DNA binding and help direct DrRecQ to specific recombination/repair sites (30).

To more accurately characterize the DNA-binding properties of BLM HRDC, we have studied the structure and DNA-binding activity of the human BLM HRDC domain by NMR spectroscopy and electrophoretic mobility shift assays (EMSAs). The BLM HRDC domain formed a bundle of five α-helices, similar to the other HRDC homologues, but had an extended acidic surface that was highly distinct from the remaining, predominantly hydrophobic surface area. BLM HRDC specifically bound to single-stranded DNA (ssDNA), mainly using its 3_{10}-helical hydrophobic loop and the N-terminal region of helix 2. In EMSAs of several BLM HRDC variants, we observed that the isolated BLM HRDC domain had quite different DNA-binding modes with ssDNA versus Holliday junction. Based on these findings, we propose that the human BLM HRDC domain may be adapted to play a distinct role in BLM that involves protein–DNA interactions.

MATERIALS AND METHODS

Cloning and protein purification

The cDNA encoding the human BLM HRDC domain (residues 1210–1294) was amplified by PCR from pJK1DNA (a kind gift from Dr Ian Hickson of Oxford University) (4) using the following two primers that were purchased from Bioneer, Inc. (Daejeon, Korea): forward (5′-GCGCATATGCAGAGG GAAGAG ATGGTT-3′) and reverse (5′-GCGCTCGAGTCAGTCTTCAGCTGG CGATGT-3′). The amplified DNA fragment was digested with Nde I and Xho I and was inserted into a pET15b plasmid encoding an N-terminal hexa-His tag fusion protein (namely, pET15b-BLMHRDC). The plasmid sequence was confirmed by DNA sequencing (Genotech, Korea). *Escherichia coli* strain BL21 (DE3) pLysS (Stratagene) was transformed with pET15b-BLMHRDC and used for protein production. Cells were grown at 37°C in Luria-Bertani (LB) broth or M9 minimal medium. For protein expression, cells were grown at 30°C and induced with 0.4 mM Isopropyl β-D-1-thiogalactopyranoside (IPTG). Isotopic labeling of all proteins was carried out by growing the cultures in modified minimal medium containing 1 g/l $^{15}NH_4Cl$ and/or 2 g/l ^{13}C-glucose as nitrogen and/or carbon sources, respectively (CIL Inc.). After cell resuspension in 25 mM Tris–HCl (pH 8.0), 500 mM NaCl, 10 mM β-mercaptoethanol and 0.2% Triton X-100, proteins were initially purified by a Ni–NTA column (Quiagen Inc.). Following dialysis of the eluted, pooled protein fractions in 25 mM Tris–HCl (pH 7.5), 100 mM NaCl and 5 mM β-mercaptoethanol, the histidine tag was removed by an overnight incubation with thrombin protease at room temperature and a second round of Ni–NTA chromatography to remove the fusion tags. Further purification of the protein was carried out using a Q Sepharose column (Amersham Biosciences) to remove nucleic acids and a HiLoad 16/60 Superdex 75 gel-filtration column (Amersham Biosciences) pre-equilibrated with buffer A (20 mM HEPES, pH 7.0, 100 mM NaCl, 1 mM DTT). The purity and homogeneity of all samples were confirmed by SDS–PAGE. For NMR measurements, the samples were concentrated to 0.8–1.2 mM in Buffer A with 1 mM EDTA and 0.02% NaN_3 (in 90% H_2O/10% D_2O or 100% D_2O) using an Amicon Ultra-15 filter (5000 MWCO, Millipore).

DNA substrates

DNA substrates purchased from Bioneer, Inc. (Daejeon, Korea) were: 1SD* (5′-GCGCATATGGAGCGTTTCC AAAGTCTTAG-3′: 29 nt) and 2DD (5′-CTAAGACTTT GGAAACGCTCCATATGCGC-3′: 29 nt). 1SD* and 2DD were used to make the double-stranded (ds) DNA substrate; 1SD* was used for the ssDNA substrate; and the synthetic HJ DNA (4X-12) consisted of four 50-nt oligonucleotides (31,32) and prepared as described by Mohaghegh *et al*. (8). The structure of the prepared HJ DNA was that of mobile HJ with a homologous core and 25 bp on each arm (8,33). For each substrate a single oligonucleotide (*) was 5′-end-labeled with [γ-^{32}P] ATP (specific activity, >3000 Ci/mmol, NEN Radiochemicals) using T4 polynucleotide kinase (Takara, Inc.) The labeled oligonucleotides were dissolved in 10 mM Tris–HCl (pH 7.5) buffer with 0.1 M NaCl and 1 mM EDTA and annealed to their unlabelled complementary strand by incubation at 95°C for 5 min and slowly cooled to room temperature for ~1 h. For purification, unincorporated label was removed by Sephadex G-50 resin. All substrates were gel purified by electrophoresis through 12% non-denaturing PAGE (37.5:1), visualized and isolated from the gel slice using the standard crash/soak method (34) of elution [10 mM Tris–HCl (pH 7.5),1 mM $MgCl_2$, 1 mM EDTA and 350 mM NaCl], followed by precipitation with EtOH. Samples were then dissolved in TEN buffer [10 mM Tris–HCl (pH 8.0), 10 mM EDTA, 50 mM NaCl].

A DNA substrate purchased from the IDT, Inc. (San Diego, CA, USA) was: 3SD-11(5′-TCATTCAGAGT-3′: 11 nt). 3SD-11 was used as the substrate for NMR titration. The purity and homogeneity of the products were confirmed by matrix-assisted laser desorption ionization mass spectroscopy. It was dialyzed into protein buffer (25 mM HEPES, pH 7.0, 100 mM NaCl and 1 mM EDTA) for 12 h. DNA concentrations were determined by measuring absorbance at 260 nm.

NMR spectroscopy and structure calculation

All NMR spectra were recorded at 298 K on a Varian INOVA 600 MHz spectrometer (KAIST, Daejon) and a Bruker AVANCE 800 MHz spectrometer (Korea

Basic Science Institute, Ochang). Backbone and side-chain assignments of human BLM HRDC were obtained by using a combination of standard triple resonance experiments (35). All spectra were processed with NMRPipe software (36) and analyzed with SPARKY3 version 3.113 software (T.D. Goddard and D.G. Kneller, SPARKY 3, University of California, San Francisco, CA, USA). Distance constraints were derived from 3D simultaneous ^{13}C- and ^{15}N-NOESY experiments acquired with a mixing time of 120 ms. Structure calculations were initially performed using CYANA program version 2.1, which combines automated assignment of NOE cross-peaks and structure calculation (37). The initial CYANA structure calculations were performed by including backbone torsion angle constraints (φ and ψ) from TALOS (38). Among the 100 independently calculated structures, the 20 conformers with the lowest CYANA target function values and that were most consistent with the experimental restraints were used for further analyses. Structures with the lowest NOE energies were retained and validated using PROCHECK (39). Structures were analyzed and visualized using PyMOL (DeLano Scientific LLC, San Carlos, CA) and MOLMOL (40).

NMR titration and backbone ^{15}N relaxation

For the NMR titration experiments, the 3SD-11 DNA substrate was added to a 0.5 mM sample of BLM HDRC domain to achieve five titration points with the protein:DNA ratios 1:0.5, 1:1, 1:1.5, 1:2, and 1:2.5. 2D HSQC spectra were recorded at each titration point. Combined ^{15}N-^{1}H chemical shift differences were calculated using the equation $\Delta\delta = [(0.125\Delta\delta N)^2 + \Delta\delta H^2]^{1/2}$.

The measurements of the nitrogen relaxation times, T_1, T_2 and ^{15}N–^{1}H NOEs were performed at 298 K for the protein alone and the DNA-bound protein on a Varian INOVA 600MHz spectrometer (41). Ten different values for the relaxation delay were used for the T_1 (delays 50, 100, 150, 200, 250, 300, 400, 500, 700 and 900 ms) and T_2 (Carr-Purcell-Meiboom-Gill mixing times 10, 30, 50, 70, 90, 110, 130, 150, 170 and 190 ms) relaxation experiments. The T_1 and T_2 values were extracted using a curve-fitting subroutine included in the Sparky program. The ^{15}N-^{1}H NOE values were calculated as the ratio of the intensities of paired ^{15}N–^{1}H correlation peaks from interleaved spectra acquired with and without ^{1}H presaturation during a recycle time of 2.5 s.

EMSA

For DNA interaction studies using the EMSA, five variants of the pET15b-BLMHRDC plasmid were made according to the site-directed mutagenesis by PCR method (42), and the sequences of these mutants were confirmed by DNA sequencing. All mutant protein samples were purified like the wild-type (WT) one and finally dialyzed in 50 mM Tris–HCl (pH 7.5) buffer with 0.1 M NaCl, 1 mM DTT and 50% glycerol. To obtain accurate protein concentrations, we measured the concentration of the HRDC variants using the BCA protein assay (Pierce, USA).

Purified human BLM HRDC variants (WT, K1227E, Y1237A, N1239D, T1243A and V1244A) were incubated with ^{32}P-labeled DNA substrates in a binding buffer of 50 mM Tris–HCl (pH 7.5), 50 mM NaCl, 0.1 g/l BSA, 1 mM DTT, 1 mM $MgCl_2$ and 4% glycerol for 25 min at 4°C. The concentrations of the proteins and the DNA substrates used in EMSA experiments are described in the figure legends. For the competition experiments, the purified human BLM HRDC variants were pre-incubated with ~50× unlabeled competitor DNA substrate in a 20 µl volume of binding buffer for 10 min on ice. End-labeled DNA probes were then added to the reaction mixtures. After incubating for 20 min, the mixtures were separated by 6% native PAGE. Prior to loading, gels were pre-run at 6.5 V/cm for 15 min, and electrophoresis was performed in 0.5× TBE (54 mM Tris borate pH 8.3, 1 mM EDTA) for 40 min to 1 h. The gel was dried onto Whatman paper and analyzed with BAS-1500 (Fuji). The concentrations of bound and free probe were quantified by the calibration tool of TINA 2.09 g software (Raytest Isotopentechnik GmbH) and fit to the equation for a single binding site (K_d = [R][P]/[RP], where [PR] is the concentration of DNA–protein complex, [P] that of protein concentration and [R] that of unbound DNA) given by Black *et al.* (43).

RESULTS

Identification and characterization of the human BLM HRDC domain

The structures of the isolated HRDC domains from *E. coli* RecQ, Sgs1 and human WRN all share a similar overall fold—a five α-helical bundle (27–29). However, it is difficult to determine domain constructs for human BLM because of its low sequence homology (<25%) to the other RecQ family members (Figure 1B). There are two reports identifying the mammalian HRDC domain by comparing its sequence homology with orthologs (28,29). From a sequence alignment with mouse, chicken and Xenopus BLM, we hypothesized that the human BLM HRDC construct should comprise residues Gln1210 to Asp1294 (Supplementary Figure S1). This construct was predicted by the ExPASy ProtParam tool (http://www.expasy.ch/tools/) to have a much lower pI (4.8) than the pH 7.0 buffer normally used in NMR experiments, which predicts a protein amenable to structural study by NMR. Over-expression of this recombinant BLM HRDC fragment in *E. coli* yielded 100 mg from 1 l LB media. The low efficiency of thrombin digestion and limited proteolysis using subtilisin indicated that this construct is very stable and structurally compact (Supplementary Figure S2). Finally, 20 and 10 mg of purified HRDC were obtained from 1 l of LB and M9 media, respectively. CD (Jasco-810) spectral analysis of the protein indicated that the fragment contains a high amount of α-helical content (Supplementary Figure S3).

Table 1. Structural statistics for human BLM HRDC domain

NOE distance restraints	
All	1146
Short range ($\|i-j\| \leq 1$)	641
Medium range ($1 < <\|i-j\| < 5$)	309
Long range ($\|i-j\| > 5$)	196
Hydrogen bonds distance restraints (n)	32
Dihedral angle constraints (n)	114
CYANA target function (Å^2)	0.89
RMSDs from the average coordinate	
Backbone atoms (N, Ca and C) (Å)	Helix only[a]: 0.35 ± 0.06
Heavy atoms (Å)	Helix only[a]: 0.97 ± 0.08
Ramachandran plot (%)	
Most favored regions	89.3
Additional allowed regions	10.3
Generously allowed regions	0.1
Disallowed regions	0.0

[a]Helix regions indicate helix 1 (aa 1211–1233), 3_{10} helix (aa 1237–1240), helix 2 (aa 1243–1252), helix 3 (aa 1257–1262), helix4 (aa 1268–1273) and helix 5 (aa 1275–1284).

Structure of the human BLM HRDC domain

We first analyzed the human BLM HRDC domain using multidimensional NMR spectroscopy. Experimental data and structural statistics are summarized in Table 1. In total, assignments of 98.8% of the main-chain and 96.4% of the side-chain atoms of residues 1210–1294 were completed. Among all the backbone resonances, only those of Phe1238 were not assigned due to resonance overlap; however, its side-chain resonances were resolved. Figure 1C represents the final 20 conformers that adopt a well-defined tertiary structure in range from residues 1210 to 1294 except for several C-terminal residues and it was refined to a root mean square deviation (RMSD) of 0.35 Å for backbone atoms. The ribbon diagram of the human BLM HRDC domain clearly shows that the BLM HRDC consists of five α-helices and one 3_{10} helix in a hydrophobic loop (Figure 1D). A search for proteins with similar configurations was carried out using the DALI search engine (44). The human BLM backbone structure was superimposable on those of *E. coli* RecQ (27), DrRecQ (30), human WRN (29) and Sgs1 (28) with RMSDs of 1.5, 1.7, 1.7 and 2.7 Å, respectively (for 74 Cα, 78 Cα, 78 Cα and 77 Cα atoms, respectively). The residues that make up the hydrophobic core of HRDC domains are represented in Figure 1E. In the case of human BLM, Leu1222, Leu1246, Leu1249 and Leu1282 are the key hydrophobic residues holding the helical bundle structure together. The identity of these core residues diverges somewhat from other RecQ family members, as does the sequence for the 3_{10} helix. Specifically, the hydrophobic core in the three other HRDC homologues consists of Leu, Leu, Met and Ile residues (Figure 1B), and the hydrophobic linker between α-helices 1 and 2 begins as 1173-VPPX-1176 in WRN, Sgs1 and *E. coli* RecQ (numbered for WRN; X is Ala, Val or Tyr) as opposed to 1235-VHYF-1238 in BLM. The secondary structure of the hydrophobic linker is divergent in the RecQ family and difficult to predict from the sequences; a loop structure is formed in Sgs1 (28), whereas a more compact 3_{10} helix is formed in *E. coli* (27) and WRN (29). The BLM HRDC structure clearly showed that BLM adopts a 3_{10} helix structure similar to that of *E. coli* RecQ and WRN. For *E. coli* HRDC, 3_{10} helix formation might be important in exposing the aromatic ring of Tyr555 to solvent for interaction with ssDNA (27). In the structure of BLM HRDC, Tyr1237 resides at the corresponding position in the hydrophobic loop.

The BLM HRDC domain contains an extended acidic surface

The electrostatic surface potential of BLM HRDC is shown in Figure 2A. The surface can almost be neatly divided into two halves, where one side of the domain is extensively negatively charged (Figure 2A, panel i), and the other is mostly neutral with a few positively charged spots (Figure 2A, panel ii). The 'top' view (Figure 2A, panel iii) shows clearly that the concentration of acidic residues is at the C-terminal end of the construct and on a surface comprising α-helices 3 to 5. Several acidic residues, including D1256, E1258, E1268, E1269, E1272, E1276 and E1288, contribute to the domain's large electronegative surface.

The pronounced electronegativity of the BLM HRDC domain has been predicted by modeling, which suggested that the function of BLM HRDC is related to protein–protein interactions (28). However, a study demonstrating the strong regulatory function of the HRDC domain in dHJ dissolution by the BLM–TOPOIIIα complex leaves a possibility for its DNA-binding ability (15). Not only that, the recently determined the crystal structure of the third HRDC domain of DrRecQ (DrRecQ HRDC #3, PDB_2RHF) shows that its highly negatively charged surface can affect DNA-binding activity and unwinding efficiency for partial duplex DNA substrates (30). In Figure 2B, we have displayed the surface charge distributions of DrRecQ HRDC #3 to compare with human BLM HRDC domain as in Figure 2A. Surface depictions of the DrRecQ HRDC #3 show a large negative surface extending from helices 1 to 5 in panel i. Panel ii shows that the DrRecQ HRDC #3 is partially hydrophobic and has positive charges around helices 1, 2 and 4. But it also has a narrow negative patch along helix 3. The top view (Figure 2B, panel iii) shows clearly that the negative surface area of DrRecQ HRDC #3 is larger than that of human BLM HRDC. Figure 2C shows the sequence similarity between human BLM and DrRecQ #3 HRDC domain using Kalign (45,46). The sequence alignment data indicates that these domains contain 13 acidic residues ranging from helices 1 to 5, although they have low sequence identity (~23%). Five acidic residues of human BLM, i.e. E1213, E1224, E1268, E1272 and E1287, are located in almost same position with D753, E760, E804, E808 and D823 of the DrRecQ HRDC #3 domain.

In our study, although the BLM HRDC domain has a net negative charge at neutral pH, the charge distribution around the hydrophobic loop is balanced, as shown in Figure 2A (panel ii). Furthermore, the sequence of the hydrophobic linker region contains a strategically placed Tyr 1237, which may facilitate DNA binding. Thus, we

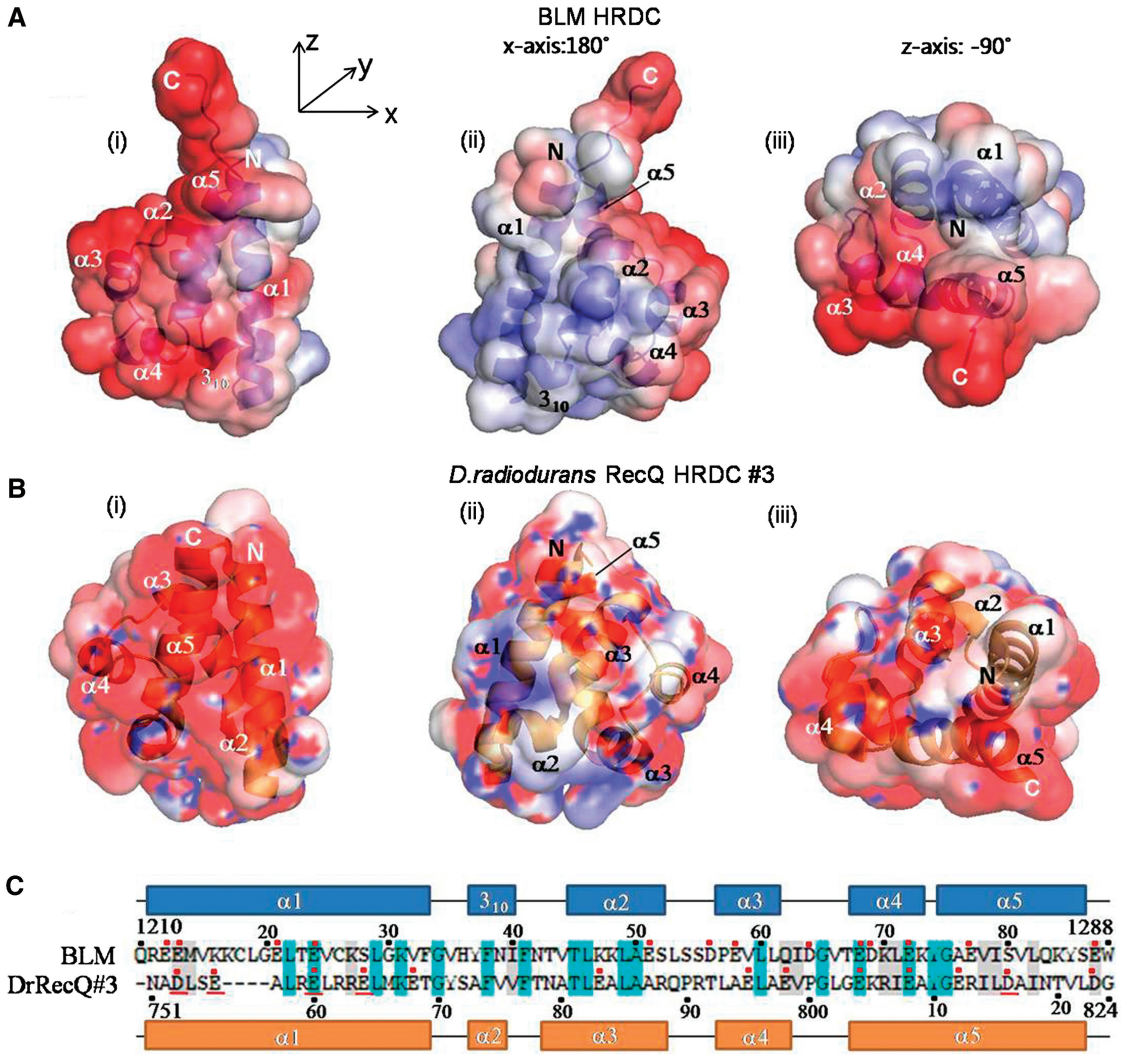

Figure 2. Comparative surface depiction between human BLM and DrRecQ HRDC #3. (**A**) Surface depiction of the human BLM HRDC domain showing the surface charge separation, with (i) an extended negative surface comprising helices 3–5, (ii) a neutral surface comprising helices 1 and 2, and (iii) the 3_{10} helical hydrophobic loop connecting them. (**B**) Surface depiction of DrRecQ HRDC #3 domain (PDB_2RHF) showing the predominant negative surface, with (i) a large negative surface covering helices 1–5, (ii) a sectional positive and neutral surface comprising helix 1 and helix 2 in hydrophobic loop and (iii) helix 4. The protein surfaces are colored by its electrostatic surface potential at ±5 kBT/*e* for positive (blue) or negative (red) charge potential using PyMol (Delano Scientific, San Carlos, CA, 2002). (**C**) Sequence alignment of the HRDC domains of BLM and DrRecQ HRDC #3 (DrRecQ#3) based on their charged residues and secondary structure. Each rectangle denotes a helix of BLM (blue) or DrRecQ#3 (orange). The identical residues are colored in cyan, and the hydrophobic and positive charged residues are colored in grey. The negative charged residues are denoted by red-colored dots and underlined acidic residues belong to the conserved acidic patch of DrRecQ HRDC #3. The helix numbering of DrRecQ is according to (30).

went on to investigate the DNA-binding ability of the BLM HRDC domain.

The human BLM HRDC domain can interact with DNA

To test whether the human BLM HRDC domain can bind to DNA, we carried out an EMSA. In these experiments, BLM HRDC was added to radiolabeled ssDNA or dsDNA substrates, and DNA bound by the domain was separated from free DNA by electrophoresis. Surprisingly, this analysis showed that the HRDC domain was able to bind to ssDNA with a K_d of ~100 μM (Figure 3A), which is almost 40 times weaker than the affinity of *E. coli* RecQ HRDC for ssDNA (27). In contrast, Figure 3B shows that the dsDNA substrate was not bound at all by the BLM HRDC domain, comparable to the results for *E. coli* RecQ HRDC (27).

To confirm the DNA-binding properties of the BLM HRDC domain, we also measured chemical shift changes in the NMR spectra of ^{15}N-labeled BLM HRDC upon addition of ssDNA (3SD-11 in 'Materials and Methods' section). Significant spectral changes were observed with increasing DNA concentration, indicating that the BLM HRDC domain interacts with ssDNA. The backbone amides of Lys1227, His1236, Tyr1237, Asn1239, Thr1243, Val1244, Leu1246, Asp1264 and Gly1265 displayed the largest chemical-shift changes (>0.042 ppm) upon addition of the ssDNA (Figure 3C). The majority

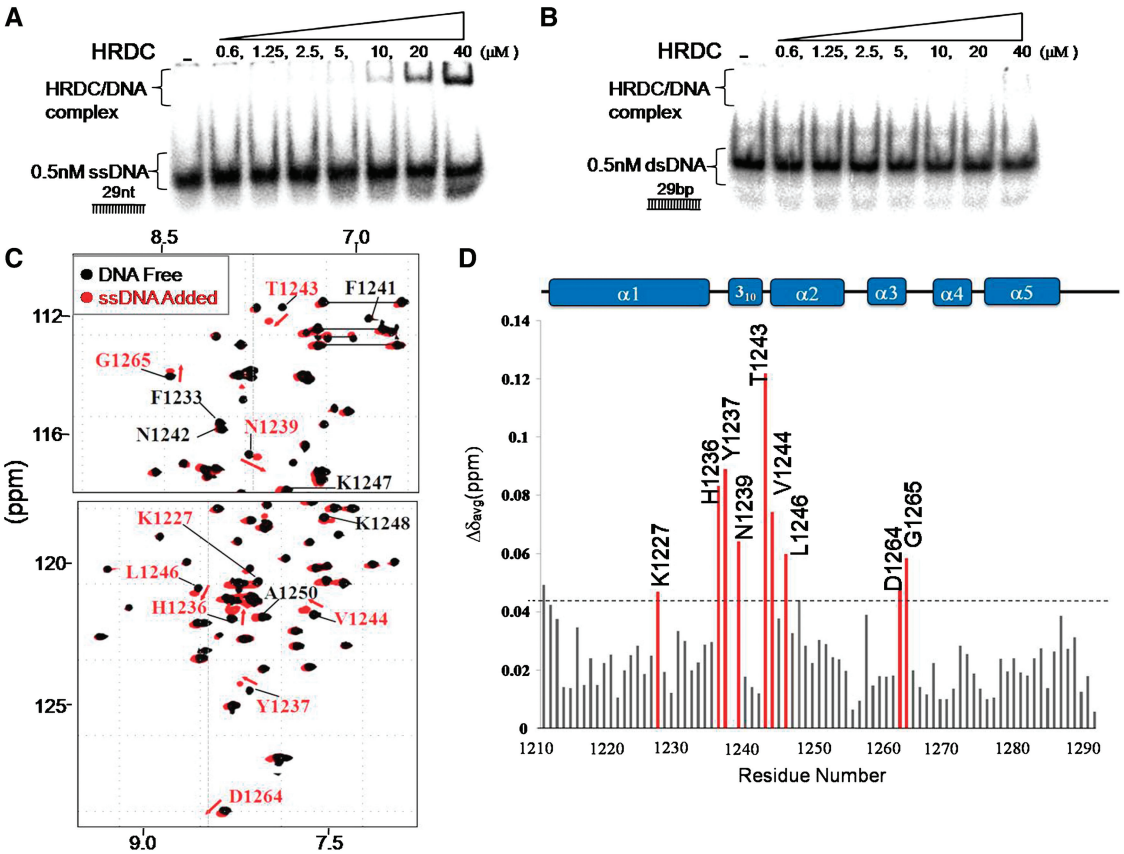

Figure 3. DNA-binding activity of the isolated human BLM HRDC domain. The BLM HRDC domain (0.6, 1.25, 2.5, 5, 10, 20 and 40 μM) was incubated with (**A**) 0.5 nM ssDNA or (**B**) 0.5 nM dsDNA. Free DNA and HRDC/DNA complexes were separated by PAGE and are indicated. Control lanes in which the HRDC domain was excluded are indicated with a '–' symbol. (**C**) Superposition of 2D ^{1}H, ^{15}N HSQC spectra of 0.5 mM ^{15}N-labeled BLM HRDC, with (red) and without (black) 1:2.5 ssDNA (3SD-11) recorded on a 600 MHz spectrometer. The perturbed residues over 0.042 ppm are indicated with red type and arrows and other positive, hydrophobic residues labeled with black type. (**D**) By-residue chemical shift perturbations of the human BLM HRDC domain upon DNA binding. Perturbations greater than 0.042 ppm are indicated by red bars. The secondary structure of BLM HRDC is shown schematically above the panel.

of the residues that underwent large changes in chemical shift were located in three regions of the BLM HRDC domain: the C-terminal end of helix 1, the 3_{10} hydrophobic loop and the N-terminal end of helix 2, and finally a short loop between helices 3 and 4 (Figure 3D).

We have indicated the DNA-binding residues of three HRDC homologues in Figure 1B. In BLM, the His1236, Tyr1237 and Asn1239 residues are three major binding residues in the hydrophobic 3_{10} helix. As mentioned above, the Tyr555 residue of *E. coli* RecQ HRDC is important for ssDNA binding (27), and is in the same structural location as Tyr1237 of BLM HRDC (Figure 1B). The Lys1227 residue in helix 1 of BLM is located similarly to a group of four ssDNA-binding residues in RecQ (28). However, the remaining ssDNA-binding residues of BLM HRDC are distinct from the other RecQ helicases. There are also differences in the distribution of basic and hydrophobic surface residues, which can easily interact with the phosphate backbone and exposed bases of the ssDNA, among the HRDC homologues.

Dynamics study of the BLM HRDC domain

The conformational equilibrium detected in the 3_{10}-helical hydrophobic loop was also observed in the NMR relaxation parameters (Figure 4). It was most clearly observed in the R_2 values, especially for Val1235, Tyr1237 and Phe1241, since they are sensitive to slower (micro- to millisecond time scale) motions. However, the R_1 values also showed significant changes in the hydrophobic loop, and particularly Tyr1237, compared to the rest of the protein sequence, in both the free HRDC and the DNA-bound complex. The average NOE values were almost the same (within the standard deviations) in the presence and absence of DNA for the 80 residues with measurable NOE relaxation data. Because of this, we conclude that the hydrophobic interaction between the BLM HRDC domain and ssDNA did not alter the overall structure of HRDC.

Exploration of DNA-binding residues for different DNA substrates

Next, we focused on the residues which are important for the DNA-binding ability of the human BLM HRDC domain to interpret the EMSA data in light of the structural data. Residues whose chemical shifts were perturbed >0.042 ppm and that were located on the surface of BLM HRDC were chosen for mutational analyses (Figure 5A). We designed seven mutant constructs of

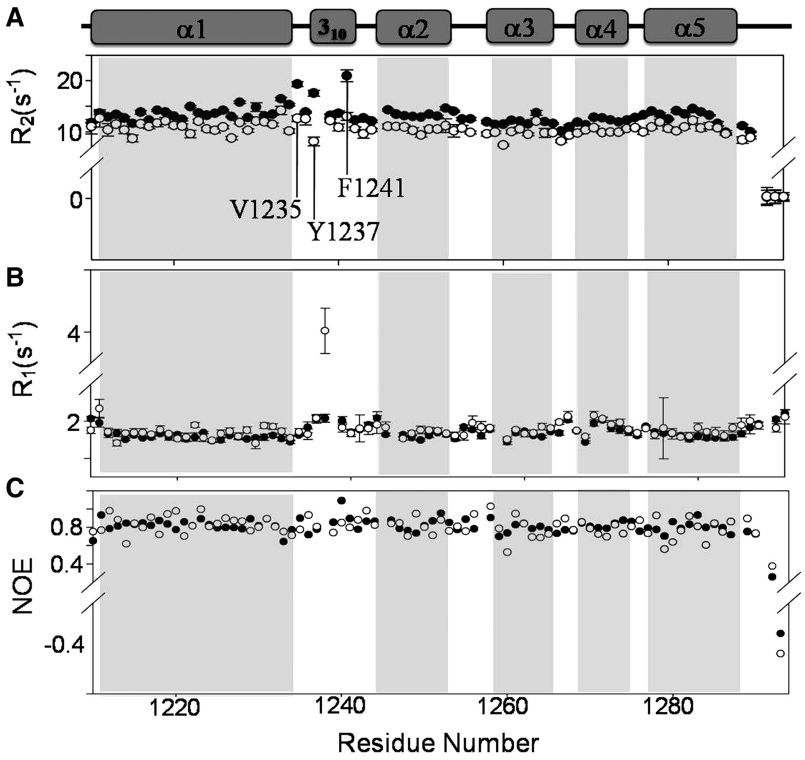

Figure 4. Backbone dynamics data for free (filled circles) and ssDNA-bound (open circles) human BLM HRDC. Residues for which resonances overlapped (Phe1238 and Trp1288) and C-terminal residues (1291–1294) are not shown. (**A**) R_2 transverse rates, (**B**) R_1 longitudinal relaxation rates and (**C**) ^{1}H-^{15}N heteronuclear NOE values. All data were collected at 600 MHz and 298 K.

HRDC: K1227E, Y1237A, N1239D, T1243A, V1244A, D1264A and G1265R (His1236 was not analyzed because its backbone resonances were not clearly visible, and Leu1246 is a hydrophobic core residue). Two of them (D1264A and G1265R) were expressed at very low levels, so we used only the remaining five HRDC variants for further studies by EMSA.

To investigate the possibility of misfolding, we selected two HRDC variants—Y1237A, which showed the largest change in R_1 and R_2 values in dynamics study, and Thr1243A, which had the largest chemical shift changes in NMR titration experiment—for measurement of 2D ^{1}H, ^{15}N-HSQC spectra in EMSA buffer (25 mM Tris–HCl (pH 7.5), 100 mM NaCl and 1 mM DTT) except for the 50% glycerol. During purification, the gel filtration results confirmed that these two HRDC variants (Y1243A and T1243A) are the same as the WT BLM HRDC and do not oligomerize in EMSA buffer (Supplementary Figure S4). And the peak sharpness and well-dispersed ^{1}H-^{15}N HSQC spectra of the HRDC variants (WT, Y1237A and T1243A) showed also that the proteins have been well folded in EMSA buffer (Figure 5B). However, surprisingly, the superposition of ^{1}H-^{15}N HSQC spectra of the three HRDC variants (WT, Y1237A and T1243A) showed clearly that several peaks in both Y1237A (red colored peaks) and T1243A (blue colored peaks) underwent large chemical shift perturbations compared to the WT spectra in EMSA buffer (Figure 5B). Because the WT BLM HRDC did not show chemical shift changes in EMSA buffer except for some of terminal residues (data not shown), we have assigned the ^{1}H-^{15}N HSQC spectra of Y1237A and T1243A based on previous assignment result. By analysis of chemical shift perturbation of Y1237A and T1243A mutant in comparison with the WT, we have mapped the locations of perturbed peaks in the structure of BLM HRDC (Supplementary Figure S5). Most of the changes in chemical shifts were concentrated in and around the 3_{10} hydrophobic loops in both Y1237A and T1243. Notably, the Y1237A mutant has a larger chemical shift change than T1243A, and its perturbations cover a wider range in the sequence (from the C-terminal end of helix 1, through the 3_{10} hydrophobic loop and the N-terminal helix 2). Most likely, these perturbations have been mainly caused by micro-environmental changes affected by the disappearance of the bulky and hydrophobic ring of Y1237, not by the severe change of protein fold (47). In Figure 5B, we display two representative residues (including the Gly1230 and Asn1239; denoted by the first and third dotted-circle from the above, respectively), which had been moved largely in both of Y1237A and T1243A mutant. We have also represented that Tyr1237 residues (the second dotted circle) were obviously disappeared in the Y1237A spectrum and also have been perturbed largely in T1243A spectrum. Interestingly, Thr1243 peak was disappeared even in Y1237A spectrum that means that two residues are structurally in reciprocal action (or effective to each other).

Figure 5C showed the differences of ssDNA-binding activity of five HRDC variants. Among the five variants

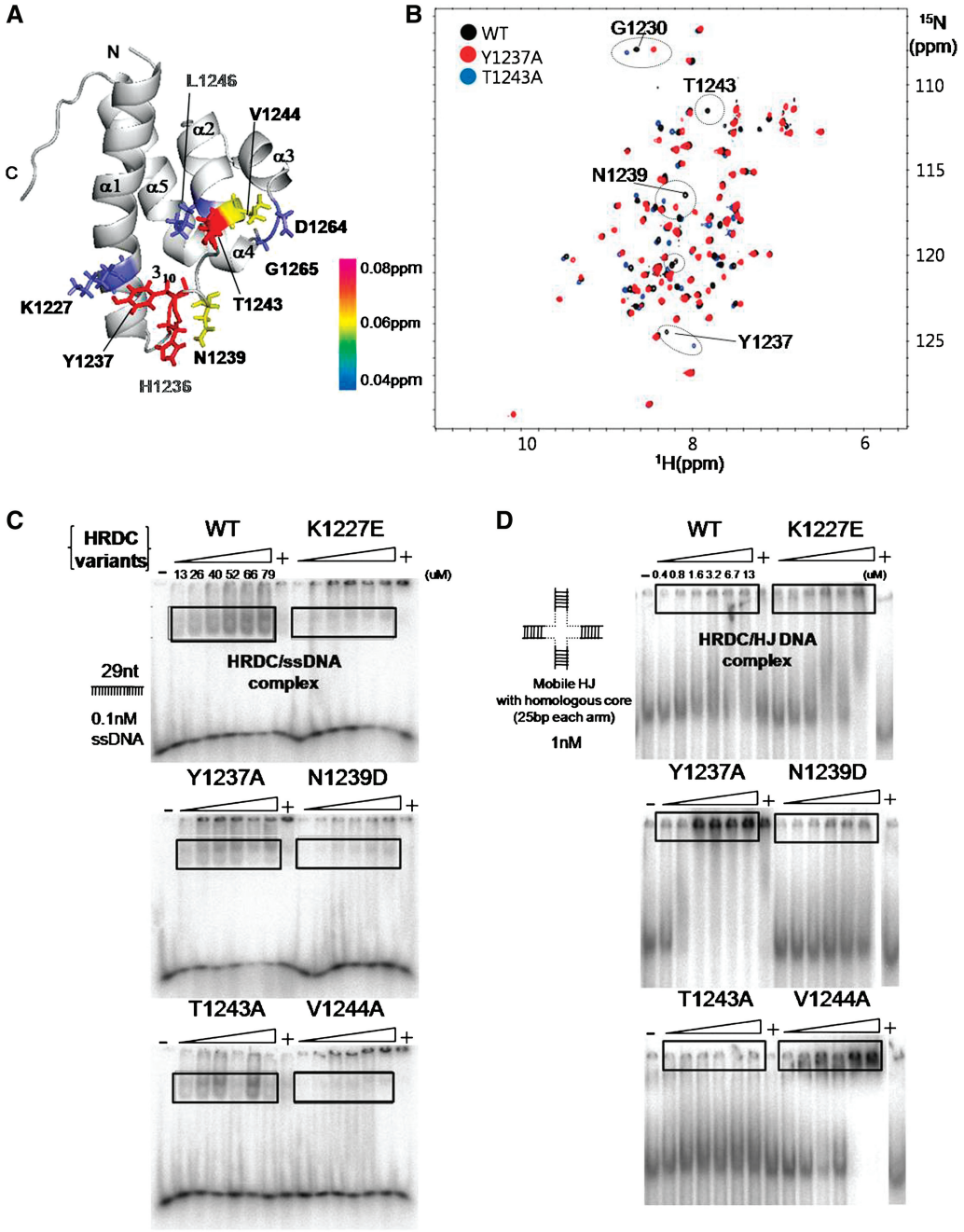

Figure 5. EMSA analysis and schematic diagram of five BLM HRDC variants involved in ssDNA and HJ DNA binding. (**A**) Ribbon diagram with chemical shift perturbations of the human BLM HRDC domain upon DNA binding. Perturbations greater than 0.04, 0.06 and 0.08 ppm are mapped onto the structure of BLM HRDC in red, yellow and blue color with side chain, respectively. Perturbed but not mutated residues (H1236 and L1246) are especially labeled in gray color. (**B**) Superposition of 2D ^{1}H, ^{15}N HSQC spectra of BLM HRDC variants (WT: black-colored peaks; Y1237A: red-colored peaks; T1243A: blue-colored peaks). The spectra were acquired by Varian INOVA 600 machine ('Materials and Methods' section: NMR spectroscopy) with 1 mM protein samples in 25 mM Tris–HCl (pH 7.5), NaCl 100 mM with 1 mM DTT at 298 K. The major perturbed residues (Gly1230:G1230, Tyr1237:Y1237, Asn1239:N1239 and Thr1243: T1243) are labeled and denoted by dashed circle. (**C**) ssDNA-binding test of each HRDC variants to 0.1 nM ssDNA. The protein concentrations were: WT: 13.2, 26.4, 39.6, 52.8, 66 and 79.2 μM; K1227E: the same concentration with WT; Y1237A: 12.6, 25.2, 37.8, 50.4, 63 and 75.6 μM; N1239D: 14.3, 28.6, 42.9, 57.2, 71.5 and 85.8 μM; T1243A: 11.9, 23.8, 35.7, 47.6, 59.5 and 71.4 μM and V1244A: 13.3, 26.6, 39.9, 53.2, 66.5 and 79.8 μM. Free DNA and HRDC variant/DNA complexes are indicated. Control lanes in which the HRDC domain was excluded are indicated with a '–' symbol, and lanes in which the 50 times non-labeled DNA was added are indicated with a '+' symbol. (**D**) HJ DNA-binding test of each HRDC variant to 1 nM HJ DNA. The protein concentration were: WT: 0.4, 0.8, 1.6, 3.2, 6.5 and 13 μM; K1227E: same concentration with WT; Y1237A: 0.4, 0.8, 1.6, 3.2, 6.3 and 12.6 μM; N1239D: 0.45, 0.9, 1.8, 3.6, 7.2 and 14.3 μM; T1243A; 0.38, 0.76, 1.5, 3.0, 6.0 and 11.9 μM and V1244A: 13.3, 0.8, 1.7, 3.3, 6.6 and 13.3 μM. Free DNA and HRDC variant/DNA complexes are indicated. To simplify the figures, we denoted the representative concentration of the WT protein for ssDNA and HJ DNA substrates. All experiments were done multiple times, and the data shown are representative.

tested, two had clear reductions in their ssDNA-binding affinities: N1239D and V1244A. The K1227E variant also showed rather weaker binding than the WT BLM HRDC. However, the Y1237A and T1243A variants retained at least nominal ssDNA affinity in compare with WT. The estimation of dissociation constants (K_d) from measuring the gel-band volumes shown in Figure 5C showed relative diffrences among five HRDC variants although they did not give clear K_d value because of very weak binding (~100 μM) (Supplementary Figure S6).

To establish whether the HRDC is a conserved HJ DNA-binding domain, we analyzed HJ DNA binding by the HRDC domain of human BLM in Figure 5D. By intensive binding tests with WT BLM HRDC for HJ DNA, we have found that the complex band of BLM HRDC-HJ DNA was the oligomerized band which could not resolve from the well. Indeed, the formation of complex band has started at even 6 μM which suggested that the HJ binding of BLM HRDC is much favorable to ssDNA. Among the variants tested, three had apparent changes in their HJ DNA-binding affinities compared to the WT domain: Y1237A, T1243A and V1244A: mutation of the conserved Thr1243 resulted in a particularly severe reduction of HJ DNA binding at high concentration. Interestingly, mutation of Tyr1237 and Val1244 led to enhancement of HJ binding that was distinguishable from the other variants and from WT BLM HRDC. This suggests that the formation of oligomers is due to an interaction between the HRDC variants and HJ DNA with different tendencies.

It is not simple to explain why the isolated BLM HRDC have different binding modes between ssDNA and HJ DNA among five HRDC variants. By the changes of the ^{1}H-^{15}N HSQC spectrum of Y1237A and T1243A mutants in Figure 5B, we could suggest that these binding differences have been caused by the combination of structural change of binding site of each HRDC variant and electro-charge changes of protein surface among them.

DISCUSSION

HRDC domains adapt for different DNA-binding modes

Since the first structural study of the Sgs1 HRDC (28) domain suggested it functioned as an auxiliary DNA-binding domain, three more crystal structure of HRDC homologues have been determined, including those from *E. coli* RecQ (27), human WRN (29) and DrRecQ (30). All HRDC domains have a very similar helical bundle structure, but they have different surface charge distributions and DNA-binding abilities. Sgs1 and *E. coli* RecQ HRDC domains bind preferentially to ssDNA over duplex DNA, whereas human WRN cannot bind even to ssDNA. In this study, we demonstrated that the isolated BLM HRDC domain also binds preferentially to ssDNA by using a binding site that includes, at minimum, Lys1227, Tyr1237, Asn1239, Thr1243 and Val1244 (Figure 6A). However, these residues form an almost entirely hydrophobic region (with the exception of the positively charged Lys1227) on the surface of BLM, making the interaction markedly weak (K_d ~100 μM) compared with *E. coli* RecQ (K_d ~2.5 μM) and Sgs1 (K_d ~30 μM). The surface diagram in Figure 6A (lower panel) depicts how mutations of these residues reduced the binding affinity of BLM HRDC for the ssDNA substrate. Mutants K1227E and N1239E produced an electronegative surface where one was not desirable, and the Tyr1237, which was the most mobile site in the dynamics study, lost a large hydrophobic surface area when changed to Ala. The binding site of *E. coli* RecQ HRDC domain, which has the strongest binding to ssDNA among the three HRDC homologues, forms a stripe that extends from the conserved hydrophobic Tyr555 along an electropositive path including Lys534, Arg543, Lys544 and Lys587 (Figure 6B). Mutation of the basic residues to Ala decreased the ssDNA-binding affinity (lower panel), demonstrating that *E. coli* HRDC needs those basic residues to recognize the phosphate backbone. The Tyr555 side chain is especially important for *E. coli* HRDC in interacting with DNA, where replacement with alanine dramatically disrupts the binding properties (27). NMR titration experiments with Sgs1 HRDC identified a similar mixture of positively charged and hydrophobic residues that make up the DNA-binding surface (Figure 6C). The binding surface is more hydrophobic than that of *E. coli* RecQ but more electropositive than BLM, and this intermediate distribution explains why the affinity of Sgs1 for ssDNA is between that of *E. coli* RecQ and human BLM (28). The human WRN HRDC was shown to lack DNA-binding ability *in vitro* despite intensive screening (14,30). The WRN HRDC domain sequence contains a lot of positive and hydrophobic residues (Figure 1E), and, as Figure 6D shows, WRN HRDC also has a positively charged region that includes Gln1165 and Lys1166 on its surface. However, many of the hydrophobic residues assemble to form a domain core, rather than being displayed on the surface of the domain. Moreover, WRN HRDC possesses additional acidic residues stacked on top of the domain (29). These differences suggest that the general HRDC domain structure is adaptable for multiple DNA-binding modes by virtue of the distribution of positive charges and hydrophobic residues on its surface. The HRDC domain can thus support specialized DNA-binding modes in different RecQ proteins.

Possible functions of the BLM HRDC domain

While the genomes of bacteria and unicellular eukaryotes typically encode a single *recQ* gene, multicellular eukaryotes express multiple *recQ* paralogs, each with specialized functions related to divergent DNA substrates. The most striking function, unique to BLM among five human RecQ helicases, is that BLM, in concert with TOPO IIIα, processes recombination intermediates containing dHJs by a process called dHJ dissolution. The dissolution is highly specific for BLM among human RecQ helicases and critically depends upon a functional HRDC domain in BLM. Furthermore, Lys1270, which is conserved from *E. coli* to humans, is predicted to play a role in mediating interactions with DNA (11). However, surprisingly, Lys1270 was not a predominant DNA-binding residue

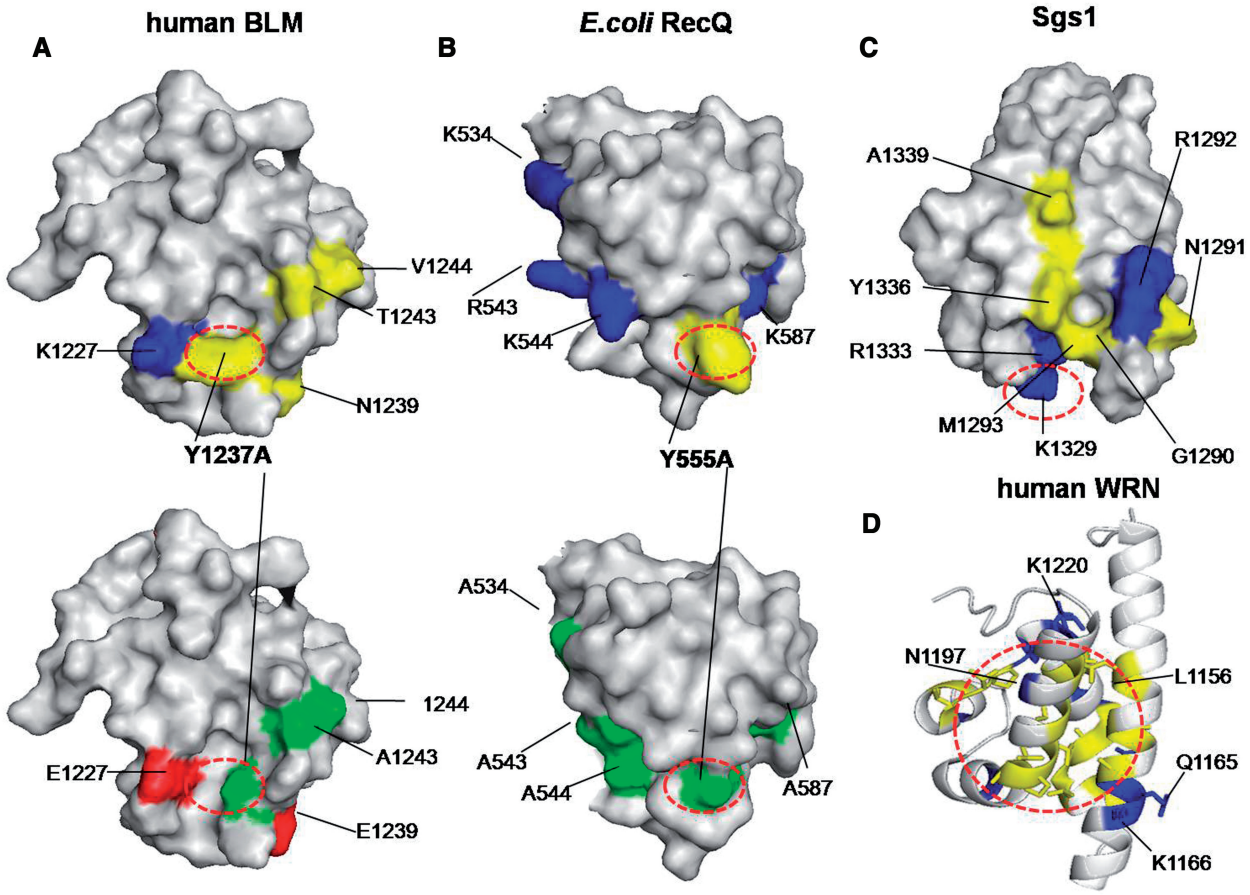

Figure 6. Comparison of ssDNA-binding residues in HRDC homologues. (**A**) Human BLM HRDC domain, (**B**) *E. coli* RecQ HRDC domain and (**C**) *S. cerevisiae* Sgs1 HRDC domain. (**D**) Ribbon diagram of human WRN HRDC domain color-coded as in surface diagrams. The protein surface is colored as follows: positive (blue), negative (red), neutral (yellow) and alanine (green).

in our ssDNA-binding study using NMR titration. In fact, Lys1270 is located in a site opposite the main ssDNA-binding groove containing the 3_{10}-helical hydrophobic loop, adjacent to a highly acidic patch including Glu1268 and Asp1269, which may explain the reason why Lys1270 was not involved in ssDNA binding (Figure 7A). Lys1270 may instead facilitate interactions with other domains in BLM. A recent study of the DrRecQ HRDC domain showed that its unusual electrostatic surface features may be important for inter-domain interactions that regulate structure-specific DNA binding and help direct DrRecQ to specific recombination/repair sites (30). The structures of *E. coli* RNaseD and *S. cerevisiae* Rrp6 further demonstrate HRDC domain specialization (48,49). These ribonuclease structures are of full-length proteins with HRDC domains and show the tenuous nature of the inter-domain interactions between their large, catalytic portions and their HRDC domains. In both structures, a single acidic residue from the HRDC domain mediates contacts with the remainder of the protein. Mutation of this acidic residue in Rrp6 altered its structure-specific nuclease activity, attesting to the importance of such inter-domain contacts. Therefore, it may be that Lys1270 of BLM HRDC has contacts with other domains in BLM, and so may modulate the enzyme activity of BLM.

However, the inter-domain model cannot explain how the single mutation of Lys1270 (K1270V) in BLM HRDC domain can reduce the efficiency of HJ DNA unwinding without compromising its catalytic efficiency for forked-duplex DNA (15). The prepared HJ DNA is a mobile HJ which have junction a 12-bp homologous core (33). The full-size BLM failed to form a stable complex with linear duplex DNA with a sequence identical to that of one of the 'arms' of the HJ DNA as well as to a similar DNA molecule of unrelated sequence, indicating that BLM specifically interacts with the crossover present in the synthetic Holliday junction (13). In this study, we have found that the isolated BLM HRDC preferentially binds to ssDNA and not dsDNA. It is altogether possible that isolated BLM HRDC domain binds to the mobile homologous junction of the prepared HJ. We hypothesize that the aggregated DNA bands in the EMSA data for HJ DNA arise from self-repulsion of HRDC, i.e. the surface charge of HRDC is not being shielded by other domains as it would be in the full-length BLM protein (Figure 7B). Interestingly, the crystal structure of the *E. coli* RuvA–HJ DNA complex indicates repulsion of HJ DNA by

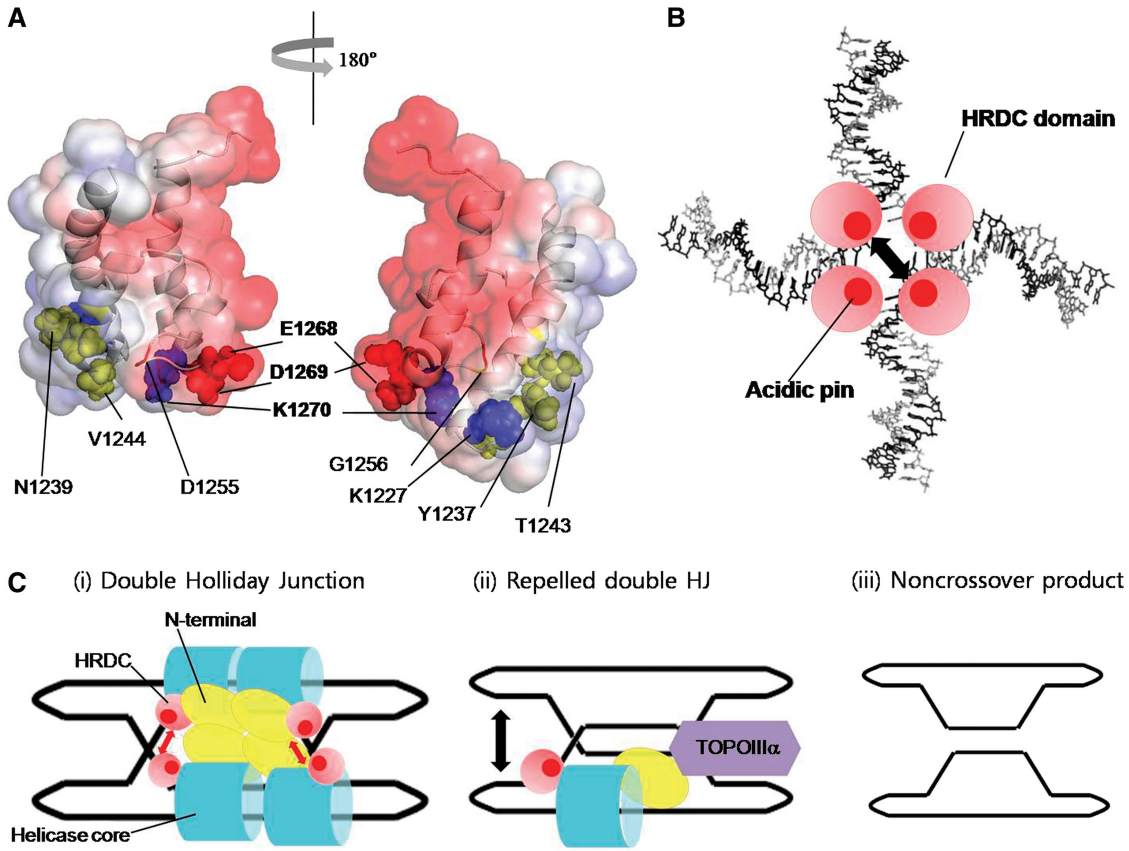

Figure 7. Electrostatic repulsion model of human BLM HRDC domain. (**A**) Diametrical views of the acidic pin motif of the human BLM HRDC domain color-coded as in Figure 1E and rendered with PyMol (Delano Scientific, San Carlos, CA, 2002). All perturbed DNA-binding residues are labeled. (B) Schematic diagram of the dissociation of BLM HRDC from HJ by electrostatic repulsion. (**C**) Mechanism of dHJ DNA dissolution by BLM–TOPOIIIα complex using electrostatic repulsion. (i) The BLM tetramer binds to dHJ DNA. The HRDC domains (red spheres) recognize the ssDNA region and the catalytic cores (blue cylinders) bind to the dsDNA region of the dHJ. The N-terminal domains are shown as yellow ellipses. (ii) The dHJ DNA is separated by electrostatic repulsion of HRDC domains and then TOPOIIIα binds to the relaxed dHJ. (iii) The TOPOIIIα resolves the dHJ DNA into non-crossover DNA.

two acidic residues of RuvA, Glu55 and Asp56 (50). In bacteria, resolution of HJs is accomplished by the RuvABC system, consisting of a junction-specific helicase complex RuvAB, which promotes branch migration, and a junction-specific endonuclease RuvC, which nicks two strands in symmetric form (51). Mutational studies of the 'acidic pin', Glu55 and Asp56, shows that mutants can modulate the branch migration rate of the RuvAB complex and markedly reduce the endonuclease activity of RuvC (50). These results suggest how important the acidic pin and electronegativity of RuvA is for binding and processing by the RuvABC resolvasome. In humans, BLM targets TOPOIIIα to its sites of action on the DNA, where DNA structures generated by the BLM helicase are required to be 'resolved' by the topoisomerase (11,14,52). On the basis of our current findings, we propose an electrostatic repulsion model to explain how these conserved acidic patches can be helpful for processing the dHJ DNA by the BLM–TOPOIIIα complex (Figure 7C). Although we cannot definitively state the oligomeric state, electron microscope (EM) images of human BLM are helpful in proposing this model. In EM imaging, BLM displays 4-fold symmetry (tetramer or octamer) and 6-fold (hexamer) symmetry *in vitro* (53). If BLM does oligomerize, it is possible that the HRDC domain from each BLM could use electrical repulsion to separate the junction sites of dHJ DNA. The BLM oligomerization is mediated by the N-terminal region (16). The BLM helicase core would preferentially bind and unwind the double stranded region of the dHJ DNA because of its higher binding affinity for dsDNA and HJ DNA (54). Then the TOPOIIIα could join the relaxed dHJ DNA–BLM complex and easily bind to the DNA product. Finally, the dHJ DNA would be divided into non-crossover products. Further investigation will be required to determine whether mutation of the acidic pin of the BLM HRDC domain can modulate the enzyme activity of BLM or the BLM–TOPOIIIα complex.

ACCESSION NUMBERS

The atomic coordinates and NMR constraints have been deposited in the RCSB Protein Data Bank under accession code rcsb101608 (PDB entry 2kv2 and BMRB accession number 16766).

SUPPLEMENTARY DATA

Supplementary Data are available at NAR Online.

ACKNOWLEDGEMENTS

We thank Dr K.-S. Ryu and E.-H. Kim for assistance with the NMR experiments. This study made use of the NMR facility at Korea Basic Science Institute, which is supported by the Bio NMR Research Program of the Korean Ministry of Science and Technology (E28070). We also thank Prof. Y.-H. Lee at the Department of Chemistry in KAIST, Korea for helping with the EMSA, and for critical discussions. Melissa Stauffer, PhD of Scientific Editing Solutions edited the manuscript.

FUNDING

This work was supported by grants 2009-0092818 and Global Research Network KRF-2009-220-C00036 to B.-S.C. from the National Research Foundation (NRF) of Korea, which is funded by the Korean government (MEST).

Conflict of interest statement. None declared.

REFERENCES

1. German,J. (1995) Bloom's syndrome. *Dermatol. Clin.*, **13**, 7–13.
2. Chaganti,R., Schonberg,S. and German,J. (1974) A manyfold increase in sister chromatid exchanges in Bloom's syndrome lymphocytes. *Proc. Natl Acad. Sci. USA*, **71**, 4508–4512.
3. Ellis,N., Lennon,D., Proytcheva,M., Alhadeff,B., Henderson,E. and German,J. (1995) Somatic intragenic recombination within the mutated locus BLM can correct the high sister-chromatid exchange phenotype of Bloom syndrome cells. *Am. J. Hum. Genet.*, **57**, 1019–1027.
4. Karow,J., Chakraverty,R. and Hickson,I. (1997) The Bloom's syndrome gene product is a 3′-5′ DNA helicase. *J. Biol. Chem.*, **272**, 30611–30614.
5. Sharma,S., Doherty,K. and Brosh,R.J. (2006) Mechanisms of RecQ helicases in pathways of DNA metabolism and maintenance of genomic stability. *Biochem. J.*, **398**, 319–337.
6. Yu,C., Oshima,J., Fu,Y., Wijsman,E., Hisama,F., Alisch,R., Matthews,S., Nakura,J., Miki,T., Ouais,S. *et al.* (1996) Positional cloning of the Werner's syndrome gene. *Science*, **272**, 258–262.
7. Kitao,S., Shimamoto,A., Goto,M., Miller,R., Smithson,W., Lindor,N. and Furuichi,Y. (1999) Mutations in RECQL4 cause a subset of cases of Rothmund-Thomson syndrome. *Nat. Genet.*, **22**, 82–84.
8. Mohaghegh,P., Karow,J., Brosh,R.J. Jr, Bohr,V. and Hickson,I. (2001) The Bloom's and Werner's syndrome proteins are DNA structure-specific helicases. *Nucleic Acids Res.*, **29**, 2843–2849.
9. Sun,H., Karow,J., Hickson,I. and Maizels,N. (1998) The Bloom's syndrome helicase unwinds G4 DNA. *J. Biol. Chem.*, **273**, 27587–27592.
10. Bachrati,C., Borts,R. and Hickson,I. (2006) Mobile D-loops are a preferred substrate for the Bloom's syndrome helicase. *Nucleic Acids Res.*, **34**, 2269–2279.
11. Wu,L. and Hickson,I. (2003) The Bloom's syndrome helicase suppresses crossing over during homologous recombination. *Nature*, **426**, 870–874.
12. Wu,L. (2008) Wrestling off RAD51: a novel role for RecQ helicases. *Bioessays*, **30**, 291–295.
13. Karow,J., Constantinou,A., Li,J., West,S. and Hickson,I. (2000) The Bloom's syndrome gene product promotes branch migration of holliday junctions. *Proc. Natl Acad. Sci. USA*, **97**, 6504–6508.
14. Wu,L., Davies,S., North,P., Goulaouic,H., Riou,J., Turley,H., Gatter,K. and Hickson,I. (2000) The Bloom's syndrome gene product interacts with topoisomerase III. *J. Biol. Chem.*, **275**, 9636–9644.
15. Wu,L., Chan,K., Ralf,C., Bernstein,D., Garcia,P., Bohr,V., Vindigni,A., Janscak,P., Keck,J. and Hickson,I. (2005) The HRDC domain of BLM is required for the dissolution of double Holliday junctions. *EMBO J.*, **24**, 2679–2687.
16. Beresten,S., Stan,R., van Brabant,A., Ye,T., Naureckiene,S. and Ellis,N. (1999) Purification of overexpressed hexahistidine-tagged BLM N431 as oligomeric complexes. *Protein Expr. Purif.*, **17**, 239–248.
17. Wu,L., Davies,S., Levitt,N. and Hickson,I. (2001) Potential role for the BLM helicase in recombinational repair via a conserved interaction with RAD51. *J. Biol. Chem.*, **276**, 19375–19381.
18. Brosh,R.J., Li,J., Kenny,M., Karow,J., Cooper,M., Kureekattil,R., Hickson,I. and Bohr,V. (2000) Replication protein A physically interacts with the Bloom's syndrome protein and stimulates its helicase activity. *J. Biol. Chem.*, **275**, 23500–23508.
19. Bernstein,D., Zittel,M. and Keck,J. (2003) High-resolution structure of the E.coli RecQ helicase catalytic core. *EMBO J.*, **22**, 4910–4921.
20. Hu,J., Feng,H., Zeng,W., Lin,G. and Xi,X. (2005) Solution structure of a multifunctional DNA- and protein-binding motif of human Werner syndrome protein. *Proc. Natl. Acad. Sci. USA*, **102**, 18379–18384.
21. Pike,A., Shrestha,B., Popuri,V., Burgess-Brown,N., Muzzolini,L., Costantini,S., Vindigni,A. and Gileadi,O. (2009) Structure of the human RECQ1 helicase reveals a putative strand-separation pin. *Proc. Natl. Acad. Sci. USA*, **106**, 1039–1044.
22. Kitano,K., Kim,S. and Hakoshima,T. (2010) Structural basis for DNA strand separation by the unconventional winged-helix domain of RecQ helicase WRN. *Structure*, **18**, 177–187.
23. Bernstein,D. and Keck,J. (2003) Domain mapping of Escherichia coli RecQ defines the roles of conserved N- and C-terminal regions in the RecQ family. *Nucleic Acids Res.*, **31**, 2778–2785.
24. Bennett,R., Sharp,J. and Wang,J. (1998) Purification and characterization of the Sgs1 DNA helicase activity of Saccharomyces cerevisiae. *J. Biol. Chem.*, **273**, 9644–9650.
25. Janscak,P., Garcia,P., Hamburger,F., Makuta,Y., Shiraishi,K., Imai,Y., Ikeda,H. and Bickle,T. (2003) Characterization and mutational analysis of the RecQ core of the bloom syndrome protein. *J. Mol. Biol.*, **330**, 29–42.
26. Morozov,V., Mushegian,A., Koonin,E. and Bork,P. (1997) A putative nucleic acid-binding domain in Bloom's and Werner's syndrome helicases. *Trends Biochem. Sci.*, **22**, 417–418.
27. Bernstein,D. and Keck,J. (2005) Conferring substrate specificity to DNA helicases: role of the RecQ HRDC domain. *Structure*, **13**, 1173–1182.
28. Liu,Z., Macias,M., Bottomley,M., Stier,G., Linge,J., Nilges,M., Bork,P. and Sattler,M. (1999) The three-dimensional structure of the HRDC domain and implications for the Werner and Bloom syndrome proteins. *Structure*, **7**, 1557–1566.
29. Kitano,K., Yoshihara,N. and Hakoshima,T. (2007) Crystal structure of the HRDC domain of human Werner syndrome protein, WRN. *J. Biol. Chem.*, **282**, 2717–2728.
30. Killoran,M. and Keck,J. (2008) Structure and function of the regulatory C-terminal HRDC domain from Deinococcus radiodurans RecQ. *Nucleic Acids Res.*, **36**, 3139–3149.
31. Lloyd,R. and Sharples,G. (1993) Processing of recombination intermediates by the RecG and RuvAB proteins of Escherichia coli. *Nucleic Acids Res.*, **21**, 1719–1725.
32. Parsons,C. and West,S. (1993) Formation of a RuvAB-Holliday junction complex in vitro. *J. Mol. Biol.*, **232**, 397–405.
33. Popuri,V., Bachrati,C., Muzzolini,L., Mosedale,G., Costantini,S., Giacomini,E., Hickson,I. and Vindigni,A. (2008) The Human RecQ helicases, BLM and RECQ1, display distinct DNA substrate specificities. *J. Biol. Chem.*, **283**, 17766–17776.
34. Sambrook,J. and Russel,D.W. (2001) *Isolation of DNA Fragments from Polyacrylamide Gels by the Crush and Soak Method: Molecular Cloning, a Laboratory Manual*. Cold Spring Harbor Laboratory Press, Cold Spring Harbor, NY.

35. Kay,L. (1997) NMR methods for the study of protein structure and dynamics. *Biochem. Cell Biol.*, **75**, 1–15.
36. Delaglio,F., Grzesiek,S., Vuister,G., Zhu,G., Pfeifer,J. and Bax,A. (1995) NMRPipe: a multidimensional spectral processing system based on UNIX pipes. *J. Biomol. NMR*, **6**, 277–293.
37. Herrmann,T., Güntert,P. and Wüthrich,K. (2002) Protein NMR structure determination with automated NOE assignment using the new software CANDID and the torsion angle dynamics algorithm DYANA. *J. Mol. Biol.*, **319**, 209–227.
38. Cornilescu,G., Delaglio,F. and Bax,A. (1999) Protein backbone angle restraints from searching a database for chemical shift and sequence homology. *J. Biomol. NMR*, **13**, 289–302.
39. Laskowski,R., Rullmannn,J., MacArthur,M., Kaptein,R. and Thornton,J. (1996) AQUA and PROCHECK-NMR: programs for checking the quality of protein structures solved by NMR. *J. Biomol. NMR*, **8**, 477–486.
40. Koradi,R., Billeter,M. and Wüthrich,K. (1996) MOLMOL: a program for display and analysis of macromolecular structures. *J. Mol. Graph.*, **14**, 29–32, 51–55.
41. Farrow,N., Muhandiram,R., Singer,A., Pascal,S., Kay,C., Gish,G., Shoelson,S., Pawson,T., Forman-Kay,J. and Kay,L. (1994) Backbone dynamics of a free and phosphopeptide-complexed Src homology 2 domain studied by ^{15}N NMR relaxation. *Biochemistry*, **33**, 5984–6003.
42. Ho,S., Hunt,H., Horton,R., Pullen,J. and Pease,L. (1989) Site-directed mutagenesis by overlap extension using the polymerase chain reaction. *Gene*, **77**, 51–59.
43. Black,D.L., Chan,R.C., Min,H., Wang,J. and Bell,L. (1997) The electrophoretic mobility shift assay for RNA binding proteins. In Smith,C.W.J. (ed.), *RNA-Protein Interactions: A Practical Approach*. Oxford University Press, Oxford, UK.
44. Holm,L. and Sander,C. (1993) Protein structure comparison by alignment of distance matrices. *J. Mol. Biol.*, **233**, 123–138.
45. Lassmann,T. and Sonnhammer,E. (2005) Kalign – an accurate and fast multiple sequence alignment algorithm. *BMC Bioinformatics*, **6**, 298.
46. Lassmann,T. and Sonnhammer,E. (2006) Kalign, Kalignvu and Mumsa: web servers for multiple sequence alignment. *Nucleic Acids Res.*, **34**, W596–W599.
47. Jung,J., Byeon,I., Wang,Y., King,J. and Gronenborn,A. (2009) The structure of the cataract-causing P23T mutant of human gammaD-crystallin exhibits distinctive local conformational and dynamic changes. *Biochemistry*, **48**, 2597–2609.
48. Zuo,Y., Wang,Y. and Malhotra,A. (2005) Crystal structure of Escherichia coli RNase D, an exoribonuclease involved in structured RNA processing. *Structure*, **13**, 973–984.
49. Midtgaard,S., Assenholt,J., Jonstrup,A., Van,L., Jensen,T. and Brodersen,D. (2006) Structure of the nuclear exosome component Rrp6p reveals an interplay between the active site and the HRDC domain. *Proc. Natl Acad. Sci. USA*, **103**, 11898–11903.
50. Ingleston,S., Sharples,G. and Lloyd,R. (2000) The acidic pin of RuvA modulates Holliday junction binding and processing by the RuvABC resolvasome. *EMBO J.*, **19**, 6266–6274.
51. West,S. (1997) Processing of recombination intermediates by the RuvABC proteins. *Annu. Rev. Genet.*, **31**, 213–244.
52. Oakley,T., Goodwin,A., Chakraverty,R. and Hickson,I. (2002) Inactivation of homologous recombination suppresses defects in topoisomerase III-deficient mutants. *DNA Repair (Amst)*, **1**, 463–482.
53. Karow,J., Newman,R., Freemont,P. and Hickson,I. (1999) Oligomeric ring structure of the Bloom's syndrome helicase. *Curr. Biol.*, **9**, 597–600.
54. Guo,R., Rigolet,P., Ren,H., Zhang,B., Zhang,X., Dou,S., Wang,P., Amor-Gueret,M. and Xi,X. (2007) Structural and functional analyses of disease-causing missense mutations in Bloom syndrome protein. *Nucleic Acids Res.*, **35**, 6297–6310.